

SCIENTIFIC REPORTS

OPEN

Sulfonated reduced graphene oxide catalyzed cyclization of hydrazides and carbon dioxide to 1,3,4-oxadiazoles under sonication

Manuri Brahmayya, Shenghong A. Dai & Shing-Yi Suen

Acid catalysts facilitate many chemical reactions. Sulfonated reduced grapheneoxide (rGOPhSO₃H) has shown to be an encouraging solid acid catalyst because of its efficiency, cost-effectiveness and safety of use. In this study, we prepared the rGOPhSO₃H nano acid catalyst, with the introduction of aromatic sulfonic acid radicals onto GO by fractional removal of oxygenated functions. It was thoroughly characterized by FT-IR, X-ray diffraction (XRD), scanning electron microscopy (SEM), transmission electron microscopy (TEM), Raman spectroscopy, energy dispersive spectroscopy (EDS) and solid state ¹³C MAS NMR (SSNMR). Here we report the conversion of CO₂ (1.0 atm pressure, at = 50 °C, the source of C₁ carbon feed stock) with hydrazides and a catalytic amount rGOPhSO₃H, which through a cyclization reaction results in a new strategy for the synthesis of 5-substituted-3H-[1,3,4]-oxadiazol-2-ones (SOxOs) under ultrasonic irradiation. Hence this concept of cyclization opens up for new insights

Synthesis of five membered 1,3,4-oxadiazoles or heterocyclic moieties elicits attention for their applications in active pharmaceutical ingredients, cell metabolism, drug intermediates, etc.¹⁻⁵. 1,3,4-oxadiazoles are especially relevant due to their predictable activity and use as significant organic intermediates in the synthesis of antibacterial, antiviral, and other drugs⁶⁻⁸. The oxidative cyclization procedure constitutes one of the most favorable ways for preparation of these significant heterocyclic rings⁹. Several metal-based heterogeneous catalysts used in oxidative cyclization methods for 1,3,4-oxadiazoles synthesis results in the emission of the poisonous gas carbon monoxide (Fig. 1a)¹⁰. In other words, the insertion of carbonyl groups into organic molecules using oxidation or hydration is generally accomplished by using transition-metal catalysts which are often expensive, hard to eliminate, poisonous, and are obtained from inadequate natural sources¹¹. Recently, we reported⁶ that carbon dioxide could effectively promote 1,3,4-oxadiazole cyclization process with hydrazides in the presence of a strong base and solvent (Fig. 1b). Still there were a few drawbacks in the reaction like, needing huge amount of solvent, strong basic medium and a long reaction times.

To seek a catalyst that covers the benefits of a metal-free and more efficient⁶ synthesis while retaining high catalytic activity, is an effort of serious importance in the preparation of 1,3,4-oxadiazoles¹²⁻¹⁴. Furthermore, solid acid catalysts have great potential to replace liquid acids, as environmentally friendly acid catalysts¹⁵⁻¹⁷. Acidic carbons, in view of green chemistry, were examined as stable and greatly active protonic acid catalysts for numerous acid catalyzed organic transformations^{18,19}. Graphene oxide, graphite oxide derivatives, and sulfonated carbon nanotubes have been meritoriously applied as advantageous heterogeneous catalysts for certain synthetic procedures²⁰⁻²⁵. Ultrasonic irradiation was applied to modify the graphite oxide and functionalized graphene oxide. Sulfonated graphene materials were recently reported for use in sonication nucleophilic substitution reactions²⁶⁻³⁰.

Herein, we report the use of sulfonated graphene oxide GOPhSO₃H, a readily obtainable, efficient and mild carbon catalyst in ultrasonic pathways. More significantly, we investigated the first application of a sulfonated nano catalyst for the direct synthesis of 1,3,4-oxadiazoles from hydrazides with easily available, inexpensive, greenhouse gas and a C1 source, carbon dioxide (1.0 MPa).

The history of graphite oxide (GO) reveals, it has functioned predominantly as a precursor to chemically enriched graphene material (CEGM) or reduced graphene oxide (r-GO), which have superior mechanical,

Department of Chemical Engineering, National Chung Hsing University, 250 KuoKuang Raod, Taichung, Taiwan, R.O.C. Correspondence and requests for materials should be addressed to S.-Y.S. (email: sysuen@dragon.nchu.edu.tw)

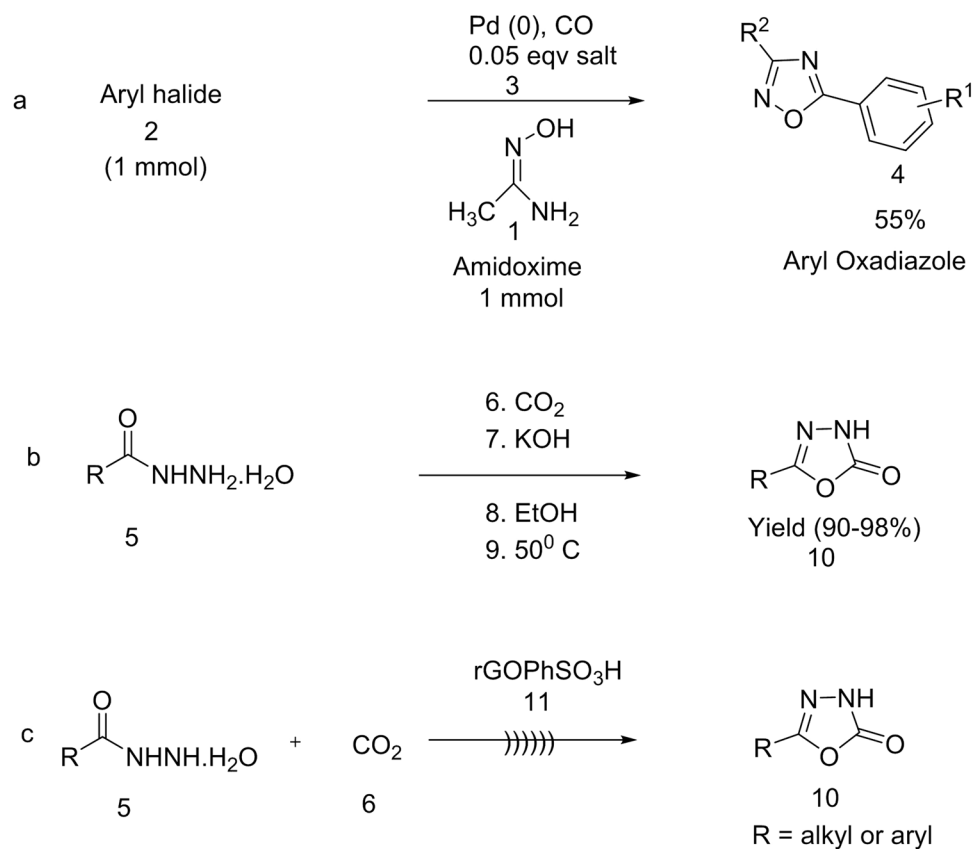


Figure 1. Previous developments of catalytic based 1,3,4-oxadiazoles with various substrates like amidoximes (a), hydrazides (b) and our current (c) synthetic applications respectively.

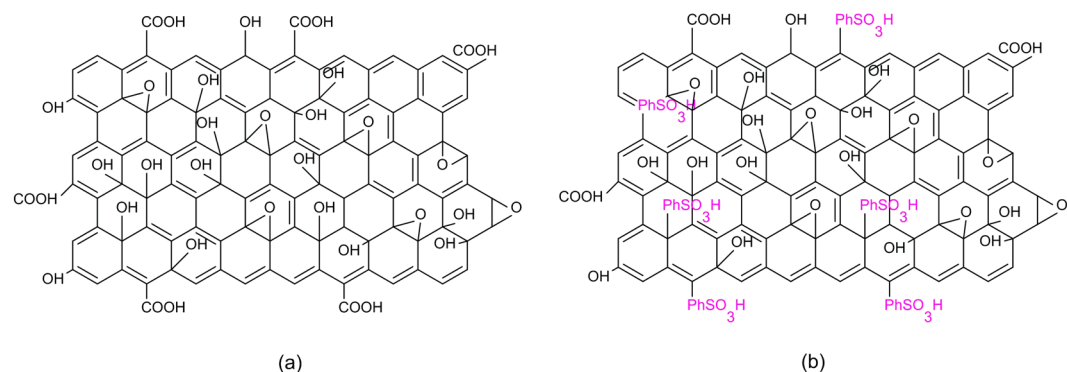


Figure 2. Model structures: (a) structural model of graphite oxide (GO) and (b) structural model of sulfonated reduced graphene oxide (rGOPhSO₃H).

chemical and electronic properties^{31–33}. The synthesis of rGO^{34,35} (Hummers method NaNO₃ and KMnO₄ in concentrated H₂SO₄) and GOPhSO₃H^{36–39} usually involves the oxidation of graphite oxide. The harsh conditions used in these synthesis procedures introduce a diversity of oxygen-containing functionalities such as alcohols, epoxides, and carboxylates onto GO^{34,40} and then conversion into GOPhSO₃H (pH 4.8 at 0.1 mgmL⁻¹)^{37,41} material (Fig. 2).

A moderate catalyst has not been discovered for enabling the production of CEGMs^{42,43}. So far, nano carbon materials have been used to improve the performance exhibited by sustained transition metal-based catalysts, e.g GO that was intact with platinum nanoparticles used in hydrogen fuel cells and in methanol electro oxidation⁴⁴. In the same way, GO imbued with palladium and silver nanoparticles exhibited very high turnover frequencies in some organic coupling reactions⁴⁵.

Results

Here, sulfonated graphene oxide was prepared by grafting sulfonic acid-containing aryl radicals onto reduced graphene oxide (rGO) (Fig. 3) under ultrasonic irradiations. The existence of countless chemical functionality

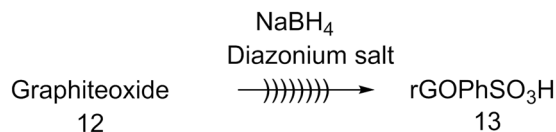


Figure 3. Synthesis of sulfonated reduced graphene oxide.

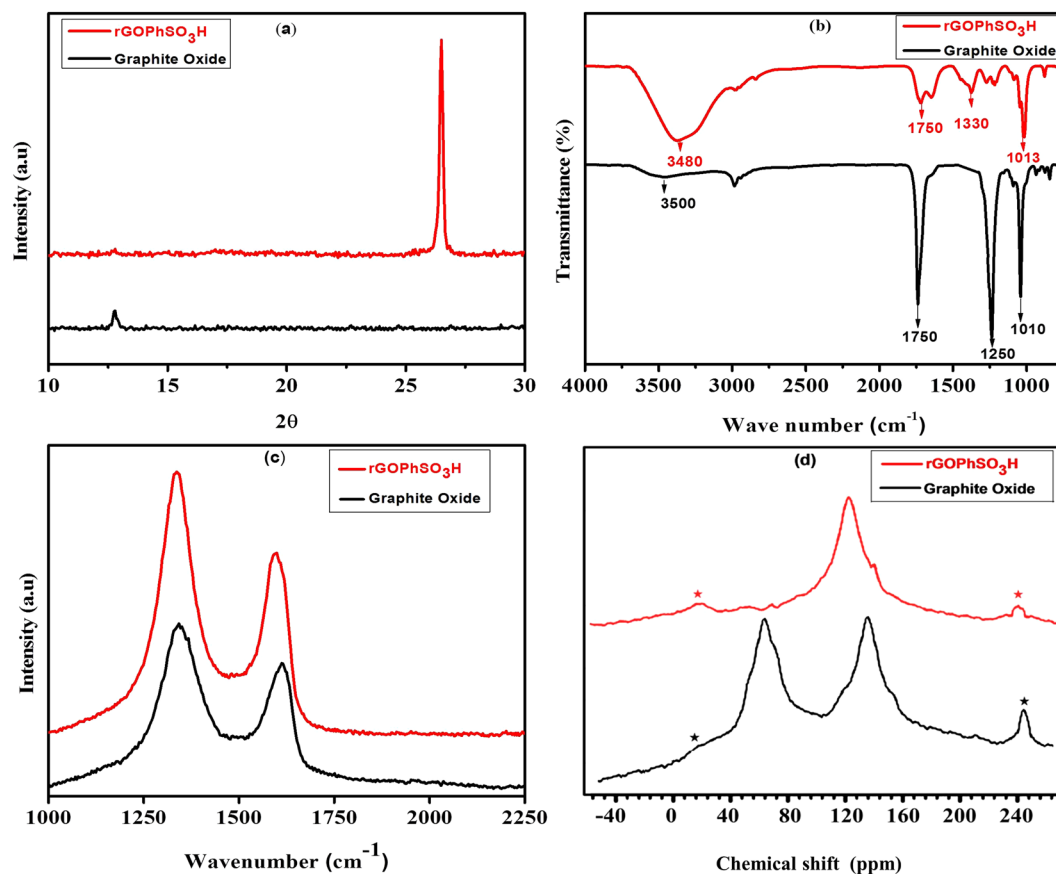


Figure 4. X-ray diffraction (b) FT-IR spectra, (c) Raman and (d) Solid state ¹³C MAS spectra of graphite oxide and sulfonated graphene oxide respectively.

on graphene oxide nano sheeted dispersion in water was studied by XRD, FTIR, Raman spectra, SEM, TEM, EDS and SSNMR. (Figure 4a) shows the XRD patterns achieved for both graphite oxide and sulfonated graphene oxide. The XRD pattern of graphite oxide exhibits a single diffraction peak at $2\theta = 12.8^\circ$ which confirms the formation of graphite upon the oxidation of graphite by the historical Hummer's procedure^{34,37,46} (Fig. 4a). After the chemical reduction of exfoliated graphene oxide with sodium borohydride and subsequent grafting of sulfonic acid containing aromatic radicals, the usual peak of graphite oxide at $2\theta = 12.8^\circ$ ($d = 6.91 \text{ \AA}$) had been shifted to $2\theta = 26.5^\circ$ ($d = 3.36 \text{ \AA}$) for rGOPhSO₃H⁴⁷ (Fig. 4a), implying that the GO nano sheets were restacked via the π - π interaction upon sulfonation.

Further, the environment of the chemical functionalities over the rGOPhSO₃H nanosheets were characterized by FTIR (Fig. 4b). A broad peak appeared at 3480 cm^{-1} , attributed to the OH bond stretching mode, and depicts the abundance of increased hydroxyl groups due to SO₃H in sulfonated graphene oxide. However, the hydroxyl groups in GO shows absorption at 3500 cm^{-1} with less intensity than rGOPhSO₃H^{37,48}. A highly sharp and strong band at 1750 cm^{-1} (ν C=O) denotes the carbonyl group and carboxylic acid observed in both GO and the obtained rGOPhSO₃H displaying the same band as highly decreased intensity, which signifies the partial reduction of graphite oxide in the sulfonation procedure. A significant peak appeared at 1330 cm^{-1} in rGOPhSO₃H, which is due to the stretching of S=O bonds and confirms the successful sulfonation that occurred on the surface of the GO⁴⁸. Furthermore, the sharp bands at 1250 cm^{-1} and 1010 cm^{-1} are ascribed to the presence of C-OH (hydroxy) and C-O (epoxy) groups, respectively in GO but the decreased band at 1013 cm^{-1} observed in rGOSO₃H nanosheets, reveals successful sulfonation.

The Raman spectra of graphite oxide and sulfonated graphene oxide (Fig. 4c) provided a significant characterization in this study. Similar to the XRD and FTIR, these spectra provided evidence that there was ample

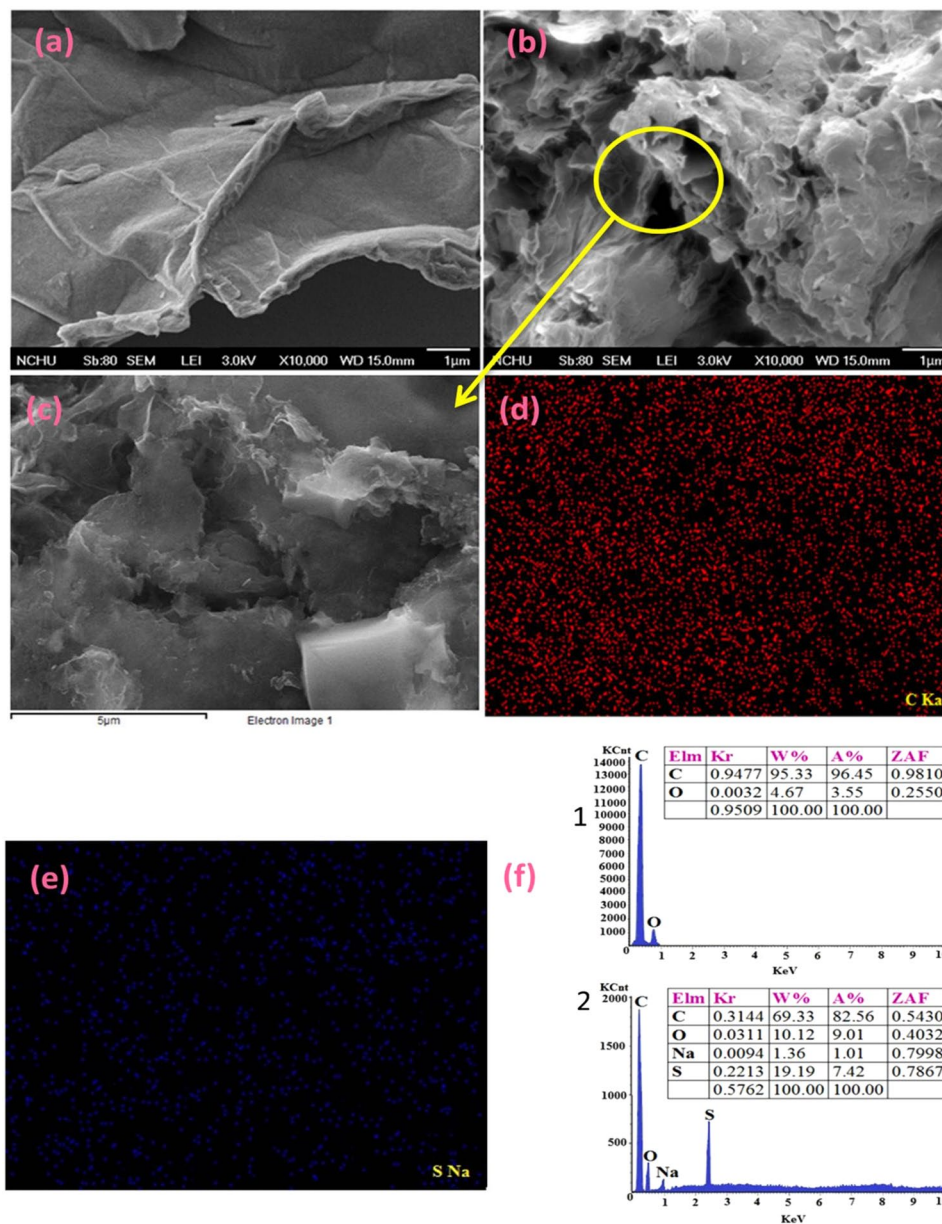


Figure 5. SEM images of (a) Graphite oxide, (b) synthesized sulfonated graphene oxide, (c) shows the SEM image of a huge area of dispersed powder of rGOPhSO₃H on the silicon wafer for elemental analysis. (d) and (e) denote the resultant EDS elemental mapping of C and S of the region which shown in (c). (f1 and f2) displays the EDS elemental analysis of graphite oxide and sulfonated graphene oxide.

presence of oxygen functionalities, such as hydroxyl, epoxide, carboxylate and carbonyl on graphite oxide, shown in (Fig. 4c). A couple of characteristic peaks at 1310 and 1593 cm^{-1} for graphite oxide and at 1312 and 1584 cm^{-1} for rGOPhSO₃H occur in each testing spectra, which corresponds to the D and G bands, respectively⁴⁹. The I_D/I_G ratio in rGOPhSO₃H (2.06) > graphite oxide (1.54). This I_D/I_G ratio difference suggests that some of the oxygenated functions are detached by NaBH₄ under the applied sonication method^{37, 45–52}.

Furthermore, the presence of morphological characteristics on the SEM images⁵³ (Fig. 5a and b) of graphite oxide and rGOPhSO₃H nanosheets confirm the successful exfoliation after embedding sulfonic acid aryl radicals onto modified rGO under ultrasonic irradiation. The EDS elemental mapping of carbon (Fig. 5d) and sulfur (Fig. 5e) in a large area (Fig. 5c) of GOPhSO₃H dispersed powder demonstrates a homogeneous distribution of PhSO₃H functionalities on the graphite oxide structure⁵³. The EDS elemental analysis (Fig. 5f1 and 5f2), reveals 69.33, 10.12, 19.19 weight% (W%) and 82.56, 9.01, 7.42 atomic % (A%) for C, O and S, respectively. Based on our sources, such high sulfur content in graphite oxide structure has not been test before. Transmission electron microscopy (TEM) confirmed⁵³ that the microstructure of the graphite oxide sheets was not damaged by the sulfonation reaction (Fig. 6). This wrinkle property may have possible benefits in acid catalyzed reactions, as the substrates can effortlessly access the active sites on both side surfaces of the 2D graphene nano sheets. Nevertheless,

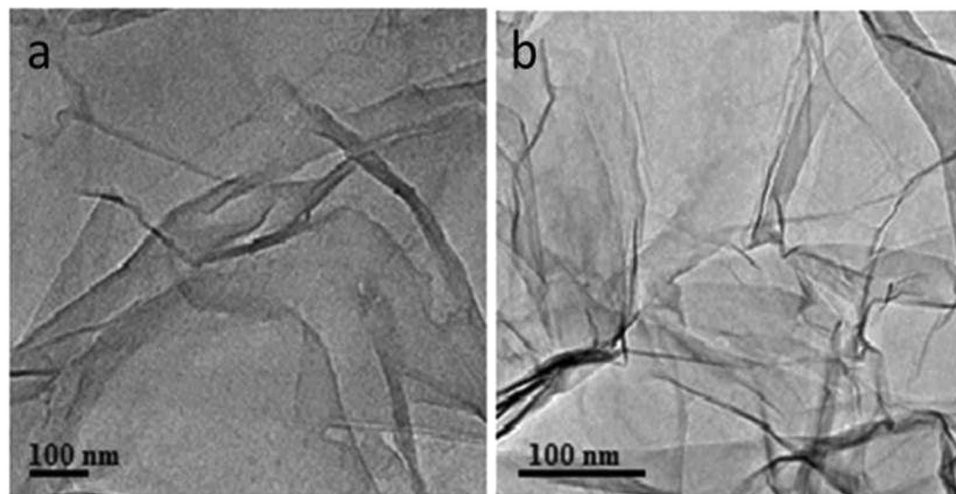


Figure 6. TEM photographs (a) graphite oxide (b) sulfonated graphene oxide.

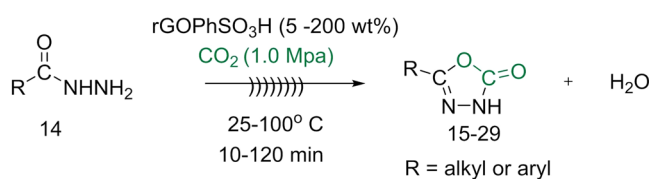
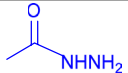
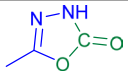
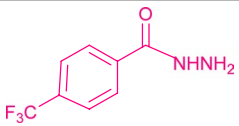
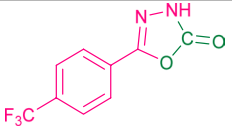
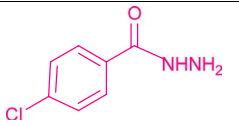
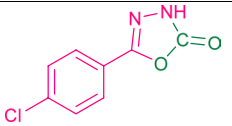
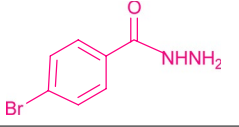
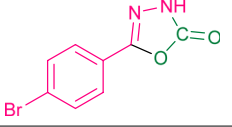
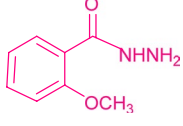
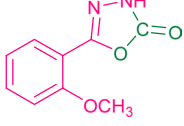
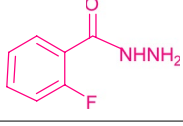
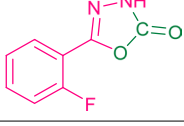
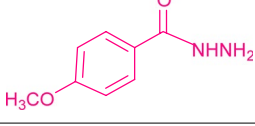
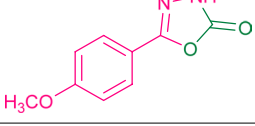
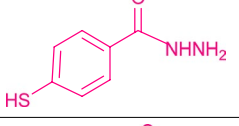
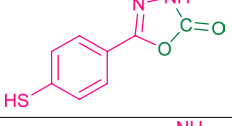
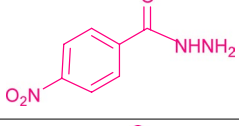
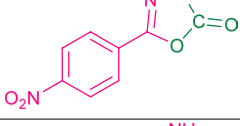
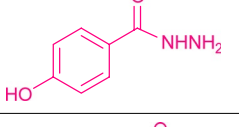
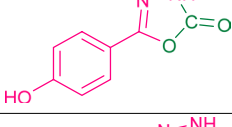
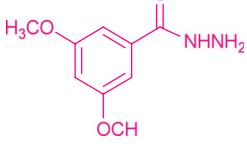
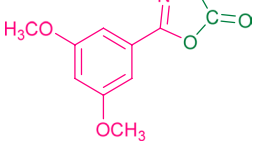
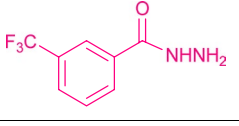
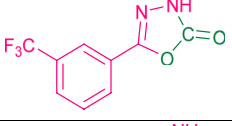
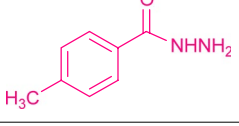
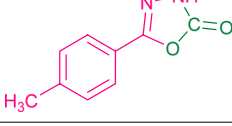


Figure 7. Synthesis of 5-substituted-1,3,4-oxadiazole-2-ones.

Catalyst	Loading [Wt%]	T (°C)	Time (Min)	Ultrasonic bath	PoxdO (Yield %)
—	—	RT ^b	48 h	—	0
—	—	50 °C	48	—	0
Graphite oxide	20	RT ^c	48 h	—	8
Graphite oxide	20	50 ^d	24 h	—	6
GOPhSO ₃ H	20	50 ^e	24 h	—	20
rGO	20	50	24 h	—	0
GOPhSO ₃ H	5	RT	10 h	Applied	70
GOPhSO ₃ H	5	50	50 min	Applied	84
GOPhSO ₃ H	5	70	50 min	Applied	76
GOPhSO ₃ H	20	RT	50 min	Applied	60
GOPhSO ₃ H	20	50	50 min	Applied	83
GOPhSO ₃ H	20	70	50 min	Applied	76
GOPhSO ₃ H	50	RT	50 min	Applied	67
GOPhSO ₃ H	50	50	50 min	Applied	88
GOPhSO ₃ H	50	70	50 min	Applied	80
GOPhSO ₃ H	200	RT	50 min	Applied	69
GOPhSO ₃ H	200	50 ^f	50 min	Applied	99
GOPhSO ₃ H	200	70	50 min	Applied	70

Table 1. Investigation of several reaction conditions for the cyclization of 4-methyl benzohydrazide with carbon dioxide into 5-phenyl-3H-[1,3,4]-oxadiazol-2-one (PoxdO)^a. (See Table S1 for further optimization studies). ^aReaction conditions: 4-methyl benzo hydrazide (1 mmol), carbon dioxide (1 atmospheric pressure), GOPhSO₃H (200 wt%). ^bblank experiment at room temperature without graphite materials and ultrasonic bath, ^{c,d}Trial experiments with graphite oxide at RT and 50 °C respectively in the absence of ultrasonic irradiation, ^eExperiment carried with sulfonated graphite oxide, under ultrasonic bath, ^fSuccessful reaction carried out using GOPhSO₃H under ultrasonication.

Entry	Hydrazide	5-substituted-1,3,4-oxadiazole-2-ones	Yield (%) ^a
15			91
16			88
17			90
18			91
19			98
20			89
21			99
22			96
23			92
24			96
25			99
26			87
27			98
Continued			

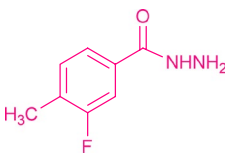
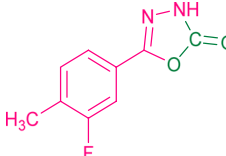
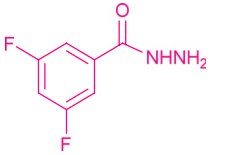
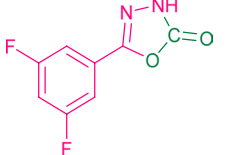
Entry	Hydrazide	5-substituted-1,3,4-oxadiazole-2-ones	Yield (%) ^a
28			94
29			86

Table 2. Ultrasound-assisted direct cyclization of various hydrazides to 5-substituted-3H-[1, 3, 4]-oxadiazole-2-ones (SOxOs) using rGOPhSO₃H nano catalyst. ^aIsolated product.

Run	1	2	3	4	5	6	7
Time (Min)	50	50	50	50	50	50	50
Yield (%) ^b	91	90	89	86	60 (90) ^c	53 (89) ^d	50(89) ^e

Table 3. Recycling experiments^a. ^aConditions as mentioned in the text, ^{b,c,d,e}The number in bracket specifies the yield of 1,3,4-oxadiazole by using the recycled acidified rGOPhSO₃H catalyst.

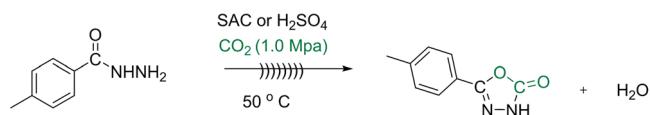


Figure 8. Synthesis of compound 27 either by using SAC or H₂SO₄.

the 2D molecular structure may be the reason for the diffusion hindrance in the reaction, the reduced sulfonated graphene nano sheets sufficiently small enough (5 μm × 1 nm in size) to be well propagated or dispersed under stirring conditions. The wrinkling facet with scarce micropores may assist the diffusion of the desired products.

Solid state ¹³C MAS NMR (SS¹³C NMR) also endorse the graphite oxide reduction (Fig. 4d). A couple of dissimilar resonances aroused in the spectrum of graphite oxide: the resonance centered at 132 ppm represents to an oxidized sp² carbons. Resonance centered at 64 ppm corresponds to epoxidation, and the 72 ppm shoulder is derived from hydroxylated carbons^{31, 54, 55}. The later weak broad resonances overlap at 158 corresponding to carbonyl carbons. The resonance peak at 132 ppm shifts to 118 ppm in rGOPhSO₃H due to the change in the chemical environs of the sp² carbons⁵⁴. The resonances at 72 ppm and 158 ppm disappear with a significant small peak roused at 142 ppm is attributed to carbons in the chemically (covalently) attached phenyl-SO₃H groups.

Discussion

Substrate scope. The catalytic potential of sulfonated graphene oxide nanosheets was examined for the cyclization of hydrazides to 1, 3, 4-oxadiazoles for the first time as shown in (Fig. 7).

In a typical experimental procedure, we examined the direct cyclization of 4-methyl benzoyl hydrazide with CO₂ under different conditions. As summarized in Table 1 (See Table S1 for the additional optimization studies) the cyclization properties of the reaction are as follows: With a neat benzohydrazide (1 mmol) and CO₂ (1.0 MPa), no reaction was observed in the absence of nano catalyst at room temperatures (RT) or 50 °C. The reaction also failed to afford the 1, 3, 4-oxadiazole moiety with the use of natural flake graphite oxide (20 wt %) at RT (48 h) and 50 °C (24 h) in conventional reaction procedure. At temperature 50 °C, in presence of synthesized nano catalyst rGOPhSO₃H the percentage conversion is at 20%, after the reaction period 24 h. Inspired by this, we tried the reaction with reproduced reduced graphene oxide^{34, 37, 40} (rGO, 20 wt%, 50 °C, 24 h) to determine its fate in cyclization procedure but unfortunately no reaction was observed. Inspired by the improved reaction yield 20% from the nano catalyst rGOPhSO₃H conventional reaction condition, we then screened our reaction possibilities under sonication. At room temperature, the percentage of the conversion hiked at 70% (10 h, with catalyst loading 5 wt %) whereas the reaction with nano catalyst (5 wt %) at 50 °C yields 84% POxDO in just 50 min (under ultrasonication). Unfortunately, the reaction yield was reduced from 84% to 76% with the same catalyst quantity at 70 °C. Maintaining the constant time factor 50 min, with various catalyst loadings (20 wt%, 50 wt%, 200 wt %) and temperatures (50 °C, 70 °C) under applied sonication bath, the best conversion of 5-phenyl-3H-[1,3,4]-Oxadiazole-2-one (POxDO) afforded (99%) at 50 °C with 200 wt% for the hydrazide vs carbon dioxide (1 mmol: P_{CO₂} = 1.0

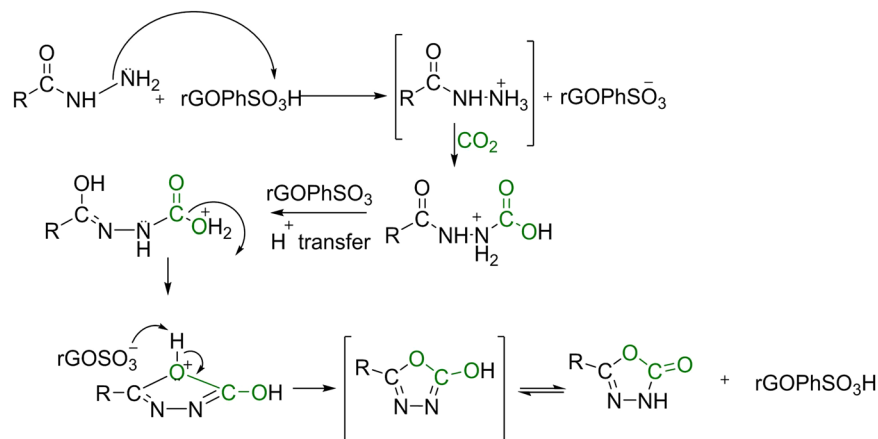


Figure 9. Postulated reaction mechanism of 5-substituted-3H-[1,3,4]-Oxadiazol-2-ones (SOxOs) under ultrasonication.

atm) rather than higher temperature 70 °C. The results summarized in Tables 1 and S1 reveals that the reaction was initiated backward for more than 50 °C with an assisted ultrasonic irradiation. This indicates that the reaction should follow the determined reaction conditions only.

Next, we expanded the possibility of the reaction by using aliphatic and aromatic hydrazides under the determined reaction conditions (Table 1) to produce the corresponding cyclized 1,3,4-oxadiazoles (Table 2). The obtained results are displayed in Table 2 (entries 15–29). All of the substrates were efficiently cyclized to the corresponding 5-substituted-3H-[1, 3, 4]-oxadiazol-2-ones [SOxOs] in tremendous yields within 50 min without generation of other waste products. Among the various hydrazides, acetohydrazide is reinforced and accelerated by +I effect⁶ and converted to 5-methyl-3H-[1,3,4]-oxadiazol-2-one (Entry 15, Table 2) i.e the flow of electrons towards the third most electronegative element nitrogen from methyl in acetohydrazide boosted up the reaction within stipulated time of sonication. As in conventional aspect, aromatic substrates with electron donating groups are readily assisting the cyclization to achieve the titled compounds (Table 2, entries 19, 21, 25, 27, 28). In the case of aromatic hydrazides that contain electrons with drawing groups, these cyclized into relatively lower yields (Table 2, entries 16, 17, 18, 20, 22, 23, 24, 26, 29) compared with their relative substrates^{3,4}. In particular, it is noteworthy to mention that thiophenol and phenol were tolerated in the reaction without need for any protecting groups in synthetically useful yields at 96% (Table 2, entries 22, 24). Thus the reaction achieved satisfactorily useful yields, even though it is slightly sensitive to substrate electronic effects. All of the obtained products were assessed by HRMS (ESI), IR & ¹HNMR, ¹³CNMR.

Recyclability of the catalyst. Additionally, we studied the recycling of the rGOPhSO₃H catalyst by selecting the reaction of 4-methoxy benzoyl hydrazide and carbon dioxide as a model reaction. Once the reaction was completed, the catalyst was easily recovered by extraction of the reaction mass with dichloromethane. The resultant aqueous layer holding catalyst was used for the subsequent experiments totaling 7 runs with the same catalyst. These experimental results are shown in Table 3. As shown, reaction time and the yield of the product was considerably found to be alike throughout the 4 reaction cycles, establishing the effective recycling of the catalyst, as well as the heterogeneous catalytic property of the established method. Yes, the reaction cycles 5–7 are evidently decreasing, which reveals that elsewhere the leaching of SO₃H function is very common problem for the sulfonated acid catalysts^{39,56}. Further advances should be made in the near future to increase the stability of the SO₃H function. It is noteworthy to explore the chemical causes for the decreased yields in the reaction cycles from 1 to 7. The leaching of SO₃H during the recycling reactions and thus the deactivation of rGOPhSO₃H may be caused by (i) decrease in the quantity of catalyst during the recycling process and (ii) the possibility of the free radical (SO₃H) substitution with substrate or mostly with hydroxy radicals under the ultrasonication⁵⁷.

On the other hand, the catalytic activity of rGOPhSO₃H was also compared with the H₂SO₄ and sulfonated active carbon (SAC) (Fig. 8). The resulting yields of compound 27 via the rGOPhSO₃H, SAC, and H₂SO₄, are 98, 45 and 38% respectively. This shows that the catalytic activity of rGOPhSO₃H is higher than with its colleague catalysts. Distinguished yields also suggest that the catalytic activity for the cyclization of substrates is not solely dependent on the catalytic acid densities but the reaction might be forwarded by the following literature reports^{58,59}. (i) accessibility of the active sites, (ii) including weakly acidic OH, COOH groups (e.g Bronsted acid sites) alongside the strongly acidic SO₃H on GO, (iii) the specific surface area of the nano catalyst and (iv) pore diameters of the prepared nano catalyst.

Influence of the sonication on the reaction. For mechanical special effects, cavitation prompted by ultrasound can support several heterogeneous and homogeneous reactions. The main principle of many claims of ultrasound is its acoustic cavitation. The generation of tiny bubbles greatly produces high pressure and heat. Key step of this application is to enhance the temperature and pressure of upto various thousand degrees (Kelvins). It is anticipated that the generated cavitation bubble delivers the needful energy for the reaction. The reaction

mechanism for direct cyclization of hydrazides with carbon dioxide using sulfonated graphene oxide catalyst under ultrasound irradiation is not very clear at this stage. Still, we proposed a reasonably plausible mechanism with our best of acquired knowledge in sonochemistry⁶⁰.

It is noteworthy to mention that the presence of phenyl sulfonated functionalities on the surface of GO plays a significant role in the activation of substrates and carbon dioxide to produce targeted oxadiazoles. The outlined mechanism is shown in (Fig. 9). The reaction initially forms of a stable hydrazide ammonium salt. This salt would be gone through a subsequent addition of carbon dioxide to release N-substituted carboxylic acid and then N-substituted carboxylate. It was anticipated that the influence of ultrasonication, higher acidic capacity of rGPhSO₃H catalyst and the increased generation of the N-Substituted carboxylate salt would force a water elimination step thereby including the 5-membered cyclization with protonated oxygen. Eventually, removal of hydrogen from the oxygen of 1, 3, 4-oxadiazole moiety to GPhSO₃⁻ anion to recycle the catalyst.

Conclusion

In summary, a simple procedure was used to prepare rGPhSO₃H nanomaterial by grafting sulfonated phenyl radicals onto the surface of rGO under ultrasound irradiation. GPhSO₃H/CO₂ was the tested system used to catalyze the cyclization involving oxidation of various hydrazides under sonochemical conditions. These results were accomplished to under mild conditions and produced 5-substituted-3H-[1, 3, 4]-oxadiazol-2-ones in outstanding yields. Additionally, recovery of catalyst was found to be both effective and convenient with use of very simple filtration procedures. These results establish the very first time a methodology to achieve 1,3,4-oxadiazoles uses a metal free carbocatalyst to support synthetically useful transformations. In a wider scope, the potentiality of rGPhSO₃H or other 2D arrays of carbon materials now covers beyond the application of their significant electronic and mechanical properties. Further developments of the reaction are under investigation.

Materials and Methods

All chemical were purchased from the local commercial sources and were used without further purification. Unless otherwise distinguished, all experiments were achieved with handy reaction conditions. ¹H and ¹³C NMR data were collected on a 400 MHz spectrometer and a 100 MHz spectrometer respectively. Chemical shift (δ) values are referenced downfield from tetramethylsilane using the residual solvent as an internal standard (All synthesized compounds were dissolved in DMSO-d₆ to analyze in NMR instruments). The mass spectra were performed by a Finnigan LTQ-Orbitrap XL instrument (ESI source). Fourier transform Infra-Red spectra were recorded with a Perkin-Elmer Spectrum One FT-IR spectrometer. X-ray diffraction was performed on MacScience MXP3 (λCu Kα = 0.154 nm) operated at 40 kV and 30 mA. The collection interval and scanning rate were 0.02° (θ/2θ mode) and 5°/min, respectively. Micro-Raman scattering experiments were achieved using a Dilor X-Y 800 spectrometer (spectral resolution of 0.6 cm⁻¹ at room temperature in air). An argon-ion laser with wavelength of 514.5 nm and with the power of 8 mW, as well as the diameter of 1 μm was used for the excitation. The spectra were performed over the wavenumber from 200 to 800 cm⁻¹ with an interval time of 600 s, and the spectra were then deconvoluted for defining the appropriate peak position. The entire spectra were standardized to the He-Ne laser excitation line. Scanning electron microscope (SEM) a model JEOL-JSM6700F instrument (Japan) was used for the morphology studies and EDX spectra. For high resolution transmission electron microscope studies, HR-TEM, model JEM-2010, JEOL, Tokyo, Japan was used. 4mm CP/MAS DR probe solid state ¹³CNMR MAS resonance spin rate at 10 KHz was used.

Preparation of sulfonated grapheneoxide (GPhSO₃H). The rGPhSO₃H nano catalyst was synthesized accordingly to a known literature³⁷⁻³⁹ procedure with minor modifications. Initially, 100 mg of graphite oxide powder was added into a glass flask with 100 ml of deionized water for 10 minutes and mixed uniformly with a magnetic stirrer at room temperature. The resulting dispersion was transferred to a vessel, and then sonicated in a ultrasonic bath (20KHz with 100% output). A solution of 0.8 g NaBH₄ in 20 mL of deionized water was slowly added dropwise into the graphene oxide dispersion, with adjusting pH of 10 by addition of 5 wt % potassium carbonate solution. Then the dispersion was heated up at 100 °C for 45 minutes during which the brown colored GO dispersion turned out as black. Later, the reaction mixture was washed with deionized water and centrifuged. The obtained incompletely reduced graphene oxide (rGO) was irradiated in 100 mL water using ultrasonic bath with a frequency of 20 kHz for 30 min and cooled. Afterwards, a diazonium salt was synthesized from the reaction of 100 mg sulfanilic acid and 1.1 mL of 1 N HCl in 15 mL water and cooled at 0 °C, monitored by adding 35 mg KNO₂ in 15 mL water. Thereafter, diazonium solution had been poured into the obtained rGO solution at 0 °C and stirred overnight 25 °C. The resulting black precipitate solution was then centrifuged at 7000 rpm for 10 min and washed five times with deionized water. The subsequent black residue was filtered under vacuum and dried in an oven at 70 °C for 4 h.

Synthetic procedure for the preparation of sulfonated active carbon. With petty modification of the previous report⁶¹, the activated-carbon (powder, 1.0 g) was taken into concentrated H₂SO₄ (18 mol L⁻¹, 25 mL) and heated under inert atmosphere 150 °C for 10 h. The obtained SAC was washed continuously (at least 6 times) with hot deionized water (2.5 L) and then with acetone, and later it was dried at 80 °C. Moreover, the achieved black powder was pre-treated hydrothermally at 200 °C for 2 h and then washed further with hot deionized water until the sulfate ions are no more eluted and detect in the washed water. Further, the density of sulfonated groups (SO₃H) on the active carbon catalyst was determined by the back acid-base titration as 1.5 mmol g⁻¹.

General procedure for the synthesis of 5-(4-methyl phenyl)-3H-[1, 3, 4]-oxadiazol-2-one by using heterogeneous sulfonated active carbon (SAC). The catalytic activities of the sulfonated active carbon were studied through the cyclization of 4-methyl benzohydrazide (MBH) with CO₂ at 50 °C. Typically, MBH (1 mmol), CO₂ (1.0 atm. pressure, at = 50 °C), and the sulfonated active carbon (SAC) catalyst (0.2 g, 1.5 mmol g⁻¹ = SO₃H) were utilized in the reaction. The reaction mass was later checked by thin layer chromatography (TLC). The achieved reaction crude was cooled to the room temperature. Then, the catalyst was separated out via the filtration and it was washed with ethanol. The obtained filtrates were subjected to evaporate under the reduced pressure to afford a residue. Thus to isolate the compound 27 (45%), afterwards it was recrystallized in EtOH.

General procedure for the synthesis of 5-(4-methyl phenyl)-3H-[1, 3, 4]-oxadiazol-2-one by using homogeneous H₂SO₄. In a 50 mL round-bottomed flask, a mixture of homogeneous H₂SO₄ (0.146 g, ρ (density) = 1.48 mmol g⁻¹), 4-methyl benzohydrazide (1 mmol) with CO₂ (1 atm. Pressure) was heated at 50 °C under ultrasonication and stirred until TLC shows the completion of the reaction. Thus, the achieved reaction mixture cooled to room temperature and extracted with ethyl acetate (2 × 5 ml) by using separating funnel. Organic layer and aqueous layers were separated. The extracted organic layer was subjected to dehydration over Na₂SO₄, filtered and vaporized under reduced pressure. Purification of the obtained sample was accomplished by column chromatography using n-hexane/EtOAc: (9:1) as an eluent to afford 38% of 5-(4-methyl phenyl)-3H-[1, 3, 4]-oxadiazol-2-one (27).

Typical procedure for the hydrazides with 1 atm. CO₂ catalyzed by rGOPhSO₃H under ultrasonication. 4-methyl benzohydrazide (1 mmol) was dissolved in ethanol (5 mL) in a 25 mL three necked round bottom (RBF) flask under ultrasonic bath with a frequency of 20 kHz and 100% output power) with a magnetic stirrer inside to mix the reaction. The reaction mixture was well stirred. Then, GOPhSO₃H (Carbocatalyst) (5–200 wt%) was added into the reaction mixture and stirred for 10 minutes to attain a homogeneous reaction mass in the flask at room temperature (RT). Carbon dioxide (1 atm) was passed into the reactor via the other available neck of the RBF with the help of the gas purging glass tube. Slowly the temperature was raised to 50 °C and was continued for 30 min. To monitor the extent of cyclization, aliquots were removed at various time intervals, mixed with DMSO-d₆ (1 mL), filtered off, to remove GOPhSO₃H, and then analyzed by NMR spectroscopy. Later, the CO₂ inlet was detached and the reactor neck was sealed and the reaction mass was refluxed for 10 minutes to achieve a complete crude product. This crude product was then quenched with dilute HCl (5%) and then 5 mL of ethyl acetate was added. The mixture was then filtered through a sintered funnel and again extracted with an ethyl acetate. The organic layer was then dehydrated over Na₂SO₄, filtered and vaporized under reduced pressure. Purification of samples was accomplished by column chromatography using n-hexane/EtOAc: (9:1) as an eluent. For NMR data charts of all compounds (compounds 15–29), see the Supplementary Information S2–S16.

Spectral Data for compounds 15–29. **5-methyl-3H-[1, 3, 4]-oxadiazol-2-one (15).** IR (KBr) ν_{max}: 2985.13, 1754.52, 1512.85, 1150.14, 1030.47 cm⁻¹. ¹HNMR (400 MHz, DMSO-d₆) δ 10.20 (brs, 1H, CONH), 2.00 (s, 3H, CH₃). ¹³CNMR (100 MHz, DMSO-d₆) 154.11, 153.63, 18.30. HRMS (ESI) calcd for [C₃H₄N₂O₂]⁺: 101.07. Found: 101.04.

5-(4-trifluoro phenyl)-3H-[1, 3, 4]-oxadiazol-2-one (16). IR (KBr) ν_{max}: 3010.39, 2976.43, 1760.00, 1489.85, 1150.14, 1100, 1011.33 cm⁻¹. ¹HNMR (400 MHz, DMSO-d₆) δ 10.47 (brs, 1H, CONH), 7.63 (dd, J = 8.0, 2H, ArH) 7.0 (dd, J = 7.4 Hz, 2H, ArH). ¹³CNMR (100 MHz, DMSO-d₆) 155.55, 154.34, 129.80, 129.00, 125.00, 124.35, 121.36. HRMS (ESI) calcd for [C₉H₆F₃N₂O₂]⁺: 231.06. Found: 231.01.

5-(4-chloro phenyl)-3H-[1, 3, 4]-oxadiazol-2-one (17). IR (KBr) ν_{max}: 3020.17, 2852.33, 1755.10, 1480.85, 1135.12, 1100, 1016.11 cm⁻¹. ¹HNMR (400 MHz, DMSO-d₆) δ 10.40 (brs, 1H, CONH), 7.66–7.80 (m, 4H, ArH). ¹³CNMR (100 MHz, DMSO-d₆) 150.36, 155.00, 154.78, 138.00, 129.01, 128.89, 128.33, 127.99, 127.32. HRMS (ESI) calcd for [C₈H₆ClN₂O₂]⁺: 197.03. Found: 197.00.

5-(4-bromo phenyl)-3H-[1, 3, 4]-oxadiazol-2-one (18). IR (KBr) ν_{max}: 3010.10, 2890.20, 1753.01, 1469.85, 1140.15, 1090, 1020.20 cm⁻¹. ¹HNMR (400 MHz, DMSO-d₆) δ 10.00 (brs, 1H, CONH), 7.64–7.80 (m, 4H, ArH). ¹³CNMR (100 MHz, DMSO-d₆) 161.00, 160.01, 138.89, 124.98, 124.00, 123.69, 123.22, 122.22. HRMS (ESI) calcd for [C₈H₆BrN₂O₂]⁺: 240.03. Found: 240.10.

5-(2-methoxy phenyl)-3H-[1, 3, 4]-oxadiazol-2-one (19). IR (KBr) ν_{max}: 3001.10, 2900.23, 1750.23, 1480.89, 1158.12, 1087, 1019.01 cm⁻¹. ¹HNMR (400 MHz, DMSO-d₆) δ 10.00 (brs, 1H, CONH), 8.2 (dd, 1H, J = 7.5 Hz, ArH), 7.8 (dd, 1H, J = 7.2 Hz, ArH), 7.45 (t, 1H, J = 6.7 Hz, ArH), 7.2 (t, 1H, J = 6.5 Hz, ArH). ¹³CNMR (100 MHz, DMSO-d₆) 150.33, 149.21, 140.00, 129.00, 126.11, 121.52, 73.00, 72.81, 72.33, 72.00, 54.69. HRMS (ESI) calcd for [C₉H₉N₂O₃]⁺: 193.13. Found: 193.11.

5-(2-fluoro phenyl)-3H-[1, 3, 4]-oxadiazol-2-one (20). IR (KBr) ν_{max}: 3030.18, 2850.00, 1757.20, 1480.88, 1150.19, 1083.00, 1000.11, 800.10 cm⁻¹. ¹HNMR (400 MHz, DMSO-d₆) δ 10.12 (brs, 1H, CONH), 7.78–8.0 (m, 4H, ArH). ¹³CNMR (100 MHz, DMSO-d₆) 163.11, 155.10, 154.67, 125.31, 124.88, 123.78, 122.65, 122.10. HRMS (ESI) calcd for [C₈H₆FN₂O₂]⁺: 181.03. Found: 181.01.

5-[4-methoxy phenyl]-3H-[1, 3, 4]-oxadiazol-2-one (21). IR (KBr) ν_{max}: 3021.03, 2894.10, 1760.10, 1479.45, 1160.30, 1075.01, 989.01, 678.66 cm⁻¹. ¹HNMR (400 MHz, DMSO-d₆) δ 10.22 (brs, 1H, CONH), 7.65–7.80 (m, 4H, ArH), 7.40–7.60 (m, 2H, ArH). ¹³CNMR (100 MHz, DMSO-d₆) 151.11, 149.79, 141.01, 121.35, 121.00, 120.35, 119.35, 114.60, 40.10. HRMS (ESI) calcd for [C₉H₉N₂O₃]⁺: 193.12. Found: 193.10.

5-(4-mercapto phenyl)-3H-[1, 3, 4]-oxadiazol-2-one (22). IR (KBr) ν_{max}: 3010.01, 2489.12, 1758.10, 1485.18, 1165.13, 1087.01, 989.31 cm⁻¹. ¹HNMR (400 MHz, DMSO-d₆) δ 10.00 (brs, 1H, CONH), 7.60–7.80 (m, 4H, ArH), 3.40 (s, 1H, ArSH). ¹³CNMR (100 MHz, DMSO-d₆) 153.21, 152.98, 128.30, 124.14, 123.34, 122.56, 122.00, 113.13. HRMS (ESI) calcd for [C₈H₇N₂O₂S]⁺: 195.05. Found: 195.03.

5-(4-nitro phenyl)-3H-[1, 3, 4]-oxadiazol-2-one (23). IR (KBr) ν_{max} : 3020.11, 1749.26, 1630 1486.38, 1157.12, 1090.02, 999.13 cm^{-1} . ^1H NMR (400 MHz, DMSO- d_6) δ 10.010 (brs, 1H, CONH), 7.25–7.45 (m, 4H, ArH). ^{13}C NMR (100 MHz, DMSO- d_6) 153.26, 139.39, 129.10, 119.23, 118.98, 113.78, 113.00. HRMS (ESI) calcd for $[\text{C}_8\text{H}_6\text{N}_3\text{O}_4]^+$: 208.07. Found: 208.00.

5-(4-hydroxy phenyl)-3H-[1, 3, 4]-oxadiazol-2-one (24). IR (KBr) ν_{max} : 3550.13, 3010.23, 1758.20, 1481.98, 1170.18, 1210.00, 1079.00, 1000.21 cm^{-1} . ^1H NMR (400 MHz, DMSO- d_6) δ 10.04 (brs, 1H, CONH), 8.8 (s, 1H, ArOH), 7.25–7.49 (m, 4H, ArH). ^{13}C NMR (100 MHz, DMSO- d_6) 154.78, 154.17, 142.33, 128.89, 128.00, 118.47, 117.33, 116.79. HRMS (ESI) calcd for $[\text{C}_8\text{H}_7\text{N}_2\text{O}_3]^+$: 179.11. Found: 179.02.

5-(3,5 dimethoxy phenyl)-3H-[1, 3, 4]-oxadiazol-2-one (25). IR (KBr) ν_{max} : 3020, 2856, 1761.11, 1485.77, 1160.20, 1084.00, 1001.11 cm^{-1} . ^1H NMR (400 MHz, DMSO- d_6) δ 10.00 (brs, 1H, CONH), 8.1 (s, 1H, J = 7.8 Hz, ArH), 7.30–7.40 (m, 2H, ArH), 3.8 (s, 6H, 2xArOCH₃). ^{13}C NMR (100 MHz, DMSO- d_6) 155.03, 154.98, 144.00, 143.79, 134.37, 118.00, 117.66, 117.00, 53.00, 52.97. HRMS (ESI) calcd for $[\text{C}_{10}\text{H}_{11}\text{N}_2\text{O}_4]^+$: 223.14. Found: 223.06.

5-(3-trifluoro phenyl)-3H-[1, 3, 4]-oxadiazol-2-one (26). IR (KBr) ν_{max} : 3019, 1753.33, 1488.89, 1159.20, 1079.00, 1060.15 cm^{-1} . ^1H NMR (400 MHz, DMSO- d_6) δ 9.89 (brs, 1H, CONH), 8.4 (m, 1H, ArH), 8.0 (m, 1H, ArH), 7.89 (s, 1H, ArH), 7.45 (m, 1H, ArH). ^{13}C NMR (100 MHz, DMSO- d_6) 155.32, 154.66, 129.10, 121.36, 121.00, 120.55, 120.00, 115.11. HRMS (ESI) calcd for $[\text{C}_9\text{H}_6\text{F}_3\text{N}_2\text{O}_2]^+$: 231.00. Found: 231.10.

5-(4-methyl phenyl)-3H-[1, 3, 4]-oxadiazol-2-one (27). IR (KBr) ν_{max} : 3018, 2859, 1760.20, 1481.11, 1153.16, 1078.23, 1010.15 cm^{-1} . ^1H NMR (400 MHz, DMSO- d_6) δ 10.10 (brs, 1H, CONH), 8.20 (d, J = 8.8 Hz, 2H, ArH), 7.88 (d, J = 8.00, 2H, ArH), 2.30 (s, 3H, ArCH₃). ^{13}C NMR (100 MHz, DMSO- d_6) 159.00, 158.30, 129.90, 122.88, 121.89, 120.98, 119.89, 112.79. HRMS (ESI) calcd for $[\text{C}_9\text{H}_9\text{N}_2\text{O}_2]^+$: 177.23. Found: 177.34.

5-(3-fluoro, 4-methyl phenyl)-3H-[1, 3, 4]-oxadiazol-2-one (28). IR (KBr) ν_{max} : 3013, 2869, 1755.44, 1486.32, 1157.16, 1081.00, 1020.19 cm^{-1} . ^1H NMR (400 MHz, DMSO- d_6) δ 10.40 (brs, 1H, CONH), 8.34 (s, 1H, ArH), 7.80 (d, 2H, J = 7.6 Hz, ArH), 7.64 (d, 1H, J = 7.4 Hz, ArH), 2.21 (s, 3H, ArCH₃). ^{13}C NMR (100 MHz, DMSO- d_6) 164.69, 150.10, 149.88, 123.22, 122.00, 121.03, 120.33, 114.23, 22.00. HRMS (ESI) calcd for $[\text{C}_9\text{H}_8\text{FN}_2\text{O}_2]^+$: 195.31. Found: 195.10.

5-(3,5-difluoro phenyl)-3H-[1, 3, 4]-oxadiazol-2-one (29). IR (KBr) ν_{max} : 3030, 1760.25, 1479.72, 1149.20, 1063.00, 1010.16 cm^{-1} . ^1H NMR (400 MHz, DMSO- d_6) δ 10.42 (brs, 1H, CONH), 8.46 (s, 1H, ArH), 8.20 (s, 2H, ArH). ^{13}C NMR (100 MHz, DMSO- d_6) 163.10, 162.89, 151.10, 150.22, 126.10, 118.15, 118.00, 117.67. HRMS (ESI) calcd for $[\text{C}_8\text{H}_5\text{F}_2\text{N}_2\text{O}_2]^+$: 199.17. Found: 199.10.

References

- Yang, Z.-Z., He, L.-N., Gao, J., Liu, A.-H. & Yu, B. Carbon dioxide utilization with C-N bond formation: carbon dioxide capture and subsequent conversion. *Energy Environ Sci* **5**, 6602–6639 (2012).
- Cui, Z.-N. *et al.* Synthesis and Fungicidal Activity of Novel 2,5-Disubstituted-1,3,4-oxadiazole Derivatives. *J Agr Food. Chem* **60**, 11649–11656 (2012).
- Rouhani, M., Ramazani, A. & Joo, S. W. Novel, fast and efficient one-pot sonochemical synthesis of 2-aryl-1,3,4-oxadiazoles. *Ultrason Sonochem* **21**, 262–267 (2014).
- Pineda de las Infantas y Villatoro M. J. *et al.* Amide-controlled, one-pot synthesis of tri-substituted purines generates structural diversity and analogues with trypanocidal activity. *Sci Rep* **5**, 9139 (2015).
- Wertz, S., Kodama, S. & Studer, A. Amination of Benzoxazoles and 1,3,4-Oxadiazoles Using 2,2,6,6-Tetramethylpiperidine-N-oxoammonium Tetrafluoroborate as an Organic Oxidant. *Angew Chem Int Ed* **50**, 11511–11515 (2011).
- Brahmayya, M., Dai, S. A. & Suen, S. Y. Synthesis of 5-substituted-3H-[1,3,4]-oxadiazol-2-one derivatives: a carbon dioxide route (CDR). *RSC Adv* **5**, 65351–65357 (2015).
- Desai, N. C., Dodiya, A. M., Rajpara, K. M. & Rupala, Y. M. Synthesis and antimicrobial screening of 1,3,4-oxadiazole and clubbed thiophene derivatives. *J Saudi Chem Soc* **18**, 255–261 (2014).
- Dawood, K. M. & Gomha, S. M. Synthesis and Anti-cancer Activity of 1,3,4-Thiadiazole and 1,3-Thiazole Derivatives Having 1,3,4-Oxadiazole Moiety. *J Heterocyclic Chem* **52**, 1400–1405 (2015).
- Wei, G., Huang, K., Ji, F., Wu, W. & Jiang, H. A facile approach to synthesize 3,5-disubstituted-1,2,4-oxadiazoles via copper-catalyzed-cascade annulation of amidines and methylarenes. *Chem Commun* **51**, 8857–8860 (2015).
- Young, J. R. & DeVita, R. J. Novel synthesis of oxadiazoles via palladium catalysis. *Tetrahedron Lett* **39**, 3931–3934 (1998).
- Kikuchi, S., Sekine, K., Ishida, T. & Yamada, T. C-C Bond Formation with Carbon Dioxide Promoted by a Silver Catalyst. *Angew Chem Int Ed* **51**, 6989–6992 (2012).
- Debnath, K., Pathak, S. & Pramanik, A. Synthesis of 5-aryl-3H-[1,3,4]oxadiazol-2-ones from N'-(chloro-aryl-methylene)-tert-butylcarbazates using basic alumina as an efficient and recyclable surface under solvent-free condition. *Tetrahedron Lett* **54**, 896–899 (2013).
- Kitano, M., Nakajima, K., Kondo, J. N., Hayashi, S. & Hara, M. Protonated Titanate Nanotubes as Solid Acid Catalyst. *J Am Chem Soc* **132**, 6622–6623 (2010).
- Yu, H., Jin, Y., Li, Z., Peng, F. & Wang, H. Synthesis and characterization of sulfonated single-walled carbon nanotubes and their performance as solid acid catalyst. *J Solid State Chem* **181**, 432–438 (2008).
- Verma, S. *et al.* Graphene oxide: an efficient and reusable carbocatalyst for aza-Michael addition of amines to activated alkenes. *Chem Commun* **47**, 12673–12675 (2011).
- Dreyer, D. R., Jia, H.-P. & Bielawski, C. W. Graphene Oxide: A Convenient Carbocatalyst for Facilitating Oxidation and Hydration Reactions. *Angew Chem Int Ed* **122**, 6965–6968 (2010).
- Liu, X.-Y. *et al.* Preparation of a Carbon-Based Solid Acid Catalyst by Sulfonating Activated Carbon in a Chemical Reduction Process. *Molecules* **15**, 7188 (2010).
- Nakajima, K. & Hara, M. Amorphous Carbon with SO₃H Groups as a Solid Brønsted Acid Catalyst. *ACS Catal* **2**, 1296–1304 (2012).
- Mayes, R. T., Fulvio, P. F., Ma, Z. & Dai, S. Phosphorylated mesoporous carbon as a solid acid catalyst. *Phys Chem Chem Phys* **13**, 2492–2494 (2011).
- Srivastava, S. K. & Pionteck, J. Recent Advances in Preparation, Structure, Properties and Applications of Graphite Oxide. *J Nanosci Nanotechnol* **15**, 1984–2000 (2015).
- Du, C. Y., Zhao, T. S. & Liang, Z. X. Sulfonation of carbon-nanotube supported platinum catalysts for polymer electrolyte fuel cells. *J Power Sources* **176**, 9–15 (2008).
- Mirza-Aghayan, M., Kashef-Azar, E. & Boukherroub, R. Graphite oxide: an efficient reagent for oxidation of alcohols under sonication. *Tetrahedron Lett* **53**, 4962–4965 (2012).

23. Mirza-Aghayan, M., Boukherroub, R., Nemati, M. & Rahimifard, M. Graphite oxide mediated oxidative aromatization of 1,4-dihydropyridines into pyridine derivatives. *Tetrahedron Lett* **53**, 2473–2475 (2012).
24. Zhu, S., Wang, J. & Fan, W. Graphene-based catalysis for biomass conversion. *Catal Sci Technol* **5**, 3845–3858 (2015).
25. Wang, R. *et al.* Graphene oxide: An effective acid catalyst for the synthesis of polyoxymethylene dimethyl ethers from methanol and trioxymethylene. *Catal Sci Technol* **6**, 993–997 (2016).
26. Maktedar, S. S., Mehetre, S. S., Singh, M. & Kale, R. K. Ultrasound irradiation: A robust approach for direct functionalization of graphene oxide with thermal and antimicrobial aspects. *Ultrason Sonochem* **21**, 1407–1416 (2014).
27. Wang, L., Wang, D., Zhang, S. & Tian, H. Synthesis and characterization of sulfonated graphene as a highly active solid acid catalyst for the ester-exchange reaction. *Catal Sci Tech* **3**, 1194–1197 (2013).
28. Zhou, J., Wang, Y., Guo, X., Mao, J. & Zhang, S. Etherification of glycerol with isobutene on sulfonated graphene: reaction and separation. *Green Chem* **16**, 4669–4679 (2014).
29. Zhao, G. *et al.* Sulfonated Graphene for Persistent Aromatic Pollutant Management. *Adv Mater* **23**, 3959–3963 (2011).
30. Melania, G. M., Alejandro, B., Diego, A. A. Pinacol rearrangement and direct nucleophilic substitution of allylic alcohols promoted by graphene oxide and graphene oxide CO₂H. *ChemCatChem*, doi:10.1002/cctc.201601362 (2017).
31. Stankovich, S. *et al.* Synthesis of graphene-based nanosheets via chemical reduction of exfoliated graphite oxide. *Carbon* **45**, 1558–1565 (2007).
32. Wang, G. *et al.* Facile Synthesis and Characterization of Graphene Nanosheets. *J Phys Chem C* **112**, 8192–8195 (2008).
33. McAllister, M. J. *et al.* Single Sheet Functionalized Graphene by Oxidation and Thermal Expansion of Graphite. *Chem Mater* **19**, 4396–4404 (2007).
34. Lerf, A., He, H., Forster, M. & Klinowski, J. Structure of Graphite Oxide Revisited. *J Phys Chem B* **102**, 4477–4482 (1998).
35. Hummers, W. S. & Offeman, R. E. Preparation of Graphitic Oxide. *J Am Chem Soc* **80**, 1339–1339 (1958).
36. Akhil, V. N. & Ganapati, D. Y. Synthesis and characterization of sulfonated carbon based graphene oxide monolith by solvothermal carbonization for esterification and unsymmetrical ether formation. *ACS Sustainable Chem Eng* **4**, 1963–1973 (2016).
37. Mirza-Aghayan, M., Molaei, T. M. & Boukherroub, R. Sulfonated reduced graphene oxide as a highly efficient catalyst for direct amidation of carboxylic acids with amines using ultrasonic irradiation. *Ultrason Sonochem* **29**, 371–379 (2016).
38. Samaneh, B., Reza, F. A., Rashid, B. Sulfonated reduced graphene oxide (RGO-SO₃H): As an efficient nanocatalyst for one-pot synthesis of 2-amino-3-cyano-7-hydroxy-4H-chromenes derivatives in water. *Polycycl Aromat Compd*, doi:10.1080/10406638.2016.1149080 (2017).
39. Hou, Q. *et al.* One-pot synthesis of sulfonated graphene oxide for efficient conversion of fructose into HMF. *RSC Adv* **6**, 104016–104024 (2016).
40. Szabo, T., Tombacz, E., Illes, E. & Dekany, I. Enhanced acidity and pH-dependent surface charge characterization of successively oxidized graphite oxides. *Carbon* **44**, 537–545 (2006).
41. Guixia, Z., Jiaying, L. & Xiangke, W. Kinetic and thermodynamic study of 1-naphthol adsorption from aqueous solution to sulfonated graphene nanosheets. *Chem Eng J* **173**, 185–190 (2011).
42. Mohsen, G., Hossein, N. & Zohreh, Z. Synthesis and anti-oxidant activity of star shape phenolic antioxidants catalyzed by acidic nanocatalyst based on reduced grapheneoxide. *Mater Sci Eng C* **71**, 709–717 (2017).
43. Mehran, G. & Marieh, G. Modification of heterogeneous catalyst: Sulfonated graphene oxide coated by SiO₂ as an efficient catalyst for Beckmann rearrangement. *Catal Commun* **87**, 70–73 (2016).
44. Seger, B. & Kamat, P. V. Electrocatalytically Active Graphene-Platinum Nanocomposites. Role of 2-D Carbon Support in PEM Fuel Cells. *J Phys Chem C* **113**, 7990–7995 (2009).
45. Scheuermann, G. M., Rumi, L., Steurer, P., Bannwarth, W. & Mulhaupt, R. Palladium Nanoparticles on Graphite Oxide and Its Functionalized Graphene Derivatives as Highly Active Catalysts for the Suzuki–Miyaura Coupling Reaction. *J Am Chem Soc* **131**, 8262–8270 (2009).
46. Mirza-Aghayan, M., Molaei, T. M. & Boukherroub, R. Palladium nanoparticles supported on reduced graphene oxide as an efficient catalyst for the reduction of benzyl alcohol compounds. *Catal Commun* **69**, 97–103 (2015).
47. Naeimi, H. & Golestanzadeh, M. Microwave-assisted synthesis of 6,6[prime or minute]-(aryl(alkyl)methylene)bis(2,4-dialkylphenol) antioxidants catalyzed by multi-sulfonated reduced graphene oxide nanosheets in water. *New J Chem* **39**, 2697–2710 (2015).
48. He, D. *et al.* Simultaneous sulfonation and reduction of graphene oxide as highly efficient supports for metal nanocatalysts. *Carbon* **66**, 312–319 (2014).
49. Ferrari, A. C. *et al.* Raman Spectrum of Graphene and Graphene Layers. *Phys Rev Lett* **97**, 187401 (2006).
50. Mohiuddin, T. M. G. *et al.* Uniaxial strain in graphene by Raman spectroscopy: peak splitting, G^a unisein parameters, and sample orientation. *Phys Rev B* **79**, 205433 (2009).
51. Lazzeri, M. & Mauri, F. Nonadiabatic Kohn Anomaly in a Doped Graphene Monolayer. *Phys Rev Lett* **97**, 266407 (2006).
52. Kudin, K. N. *et al.* Raman Spectra of Graphite Oxide and Functionalized Graphene Sheets. *Nano Lett.* **8**, 36–41 (2008).
53. Junyi, J. *et al.* Sulfonated graphene as water-tolerant solid acid catalyst. *Chem Sci* **2**, 484–487 (2011).
54. Titelman, G. I. *et al.* Characteristics and microstructure of aqueous colloidal dispersions of graphite oxide. *Carbon* **43**, 641–649 (2005).
55. Hontoria-Lucas. *et al.* Study of oxygen-containing groups in a series of graphite oxides: Physical and chemical characterization. *Carbon* **33**, 1585–1592 (1995).
56. Duckhee, L. Preparation of sulfonated carbonaceous material from lignosulfonate and its usefulness as an esterification catalyst. *Molecules* **18**, 8168–8180 (2013).
57. Subash, G. & Aniruddha, B. P. Modeling the effect of carbon-dioxide gas on cavitation. *Ultrason Sonochem* **34**, 721–728 (2017).
58. Wu, Y. *et al.* Microwave-assisted hydrolysis of crystalline cellulose catalyzed by biomass char sulfonic acids. *Green Chem* **12**, 696–700 (2010).
59. Pravin, P. U. *et al.* Chemical conversion of biomass-derived hexose sugars to levulinic acid over sulfonic acid-functionalized graphene oxide catalysts. *Green Chem* **15**, 2935–2943 (2013).
60. Wang, M.-L., Brahmayya, M. & Hsieh, Y.-M. The novel synthetic route of 3,5-dimethyl-1-(3-phenylpropyl)-1H-pyrazole under solid–liquid phase transfer catalysis conditions assisted by an ultrasound application—A study of some kinetic parameters. *J. Taiwan. Inst. Chem Eng.* **57**, 54–61 (2015).
61. Ayumu, O., Takafumi, O. & Kazumichi, Y. Selective hydrolysis of cellulose into glucose over solid acid catalysts. *Green Chem* **10**, 1033–1037 (2008).

Acknowledgements

The authors are thankful to the Ministry of Science and Technology in Taiwan for the financial assistance (Project numbers MOST 104-2221-E-005-064-MY3 and MOST 105-2811-E-005-008).

Author Contributions

All the three authors Manuri Brahmayya, Shenghong A. Dai, Shing-Yi Suen are equally contributed. M.B. and S.Y.S. designed research; M.B. completed experimental work and well characterized; M.B. and S.A.D. confirmed

and analyzed NMR section; S.Y.S. and M.B. analyzed the nano catalyst. S.A.D. well contributed to discussions, M.B. wrote paper under the supervision of S.A.D. and S.Y.S. All the authors reviewed the manuscript.

Additional Information

Supplementary information accompanies this paper at doi:[10.1038/s41598-017-04143-4](https://doi.org/10.1038/s41598-017-04143-4)

Competing Interests: The authors declare that they have no competing interests.

Publisher's note: Springer Nature remains neutral with regard to jurisdictional claims in published maps and institutional affiliations.



Open Access This article is licensed under a Creative Commons Attribution 4.0 International License, which permits use, sharing, adaptation, distribution and reproduction in any medium or format, as long as you give appropriate credit to the original author(s) and the source, provide a link to the Creative Commons license, and indicate if changes were made. The images or other third party material in this article are included in the article's Creative Commons license, unless indicated otherwise in a credit line to the material. If material is not included in the article's Creative Commons license and your intended use is not permitted by statutory regulation or exceeds the permitted use, you will need to obtain permission directly from the copyright holder. To view a copy of this license, visit <http://creativecommons.org/licenses/by/4.0/>.

© The Author(s) 2017